ESD-TR-91-245

AD-A250 878

(2)

Technical Report
947

Beam and Filter Straddle Losses in an ESA Search Radar

DTIC
ELECTE
JUN 0 2 1992
S B D

R.J. Galejs
C.E. Muehe

31 March 1992

Lincoln Laboratory
MASSACHUSETTS INSTITUTE OF TECHNOLOGY
LEXINGTON, MASSACHUSETTS

Prepared for the Department of the Navy under Air Force Contract F19628-90-C-0002.

Approved for public release; distribution is unlimited.

92-14235

This report is based on studies performed at Lincoln Laboratory, a center for research operated by Massachusetts Institute of Technology. The work was sponsored by the Department of the Navy under Air Force Contract F19628-90-C-0002.

The ESD Public Affairs Office has reviewed this report, and it is releasable to the National Technical Information Service, where it will be available to the general public, including foreign nationals.

This report may be reproduced to satisfy needs of U.S. Government agencies.

FOR THE COMMANDER

Hugh L. Southall

Hugh L. Southall, Lt. Col., USAF
Chief, ESD Lincoln Laboratory Project Office

Non-Lincoln Recipients

PLEASE DO NOT RETURN

Permission is given to destroy this document when it is no longer needed.

REPORT DOCUMENTATION PAGE

Form Approved
OMB No. 0704-0188

Public reporting burden for this collection of information is estimated to average 1 hour per response, including the time for reviewing instructions, searching existing data sources, gathering and maintaining the data needed, and completing and reviewing the collection of information. Send comments regarding this burden estimate or any other aspect of this collection of information, including suggestions for reducing this burden, to Washington Headquarters Services, Directorate for Information Operations and Reports, 1215 Jefferson Davis Highway, Suite 1204, Arlington, VA 22202-4302, and to the Office of Management and Budget, Paperwork Reduction Project (0704-0188), Washington, DC 20503.

1. AGENCY USE ONLY (*Leave blank*)	2. REPORT DATE	3. REPORT TYPE AND DATES COVERED
	31 March 1992	Technical Report

4. TITLE AND SUBTITLE

Beam and Filter Straddle Losses in an ESA Search Radar

5. FUNDING NUMBERS

C — F19628-90-C-0002
PE — 63103N, 62712N
PR — 401

6. AUTHOR(S)

R.J. Galejs and C.E. Muehe

7. PERFORMING ORGANIZATION NAME(S) AND ADDRESS(ES)

Lincoln Laboratory, MIT
P.O. Box 73
Lexington, MA 02173-9108

8. PERFORMING ORGANIZATION REPORT NUMBER

TR-947

9. SPONSORING/MONITORING AGENCY NAME(S) AND ADDRESS(ES)

Naval AAW Technology
Office of Naval Techn ology
800 N. Quincy Street
Arlington, VA 22202

10. SPONSORING/MONITORING AGENCY REPORT NUMBER

ESD-TR-91-245

11. SUPPLEMENTARY NOTES

None

12a. DISTRIBUTION/AVAILABILITY STATEMENT

Approved for public release; distribution is unlimited.

12b. DISTRIBUTION CODE

13. ABSTRACT (*Maximum 200 words*)

The present study was undertaken to quantify several types of losses encountered when using an electronically scanned array (ESA). The losses examined include beam straddle losses, eclipsing losses, and range-Doppler straddling losses. The losses were studied for volume search radars with square and hexagonal search patterns as well as horizon search radar.

The radar search equations for an ESA radar for both volume and horizon search are first derived. The beam straddle loss is then found, including the effect of range eclipsing for a high pulse repetition frequency (PRF) radar. The hexagonal search pattern has about 0.5 to 1 dB less loss than the square search. This loss is a strong function of probability of detection and duty factor precluding the insertion of a constant loss term in the radar range equation for these effects. A derivation of range and Doppler straddling losses follows, showing that they vary only slightly with the probability of detection and thus can be represented by a constant depending only on range-gate and Doppler-filter spacings. All losses were found to be very insensitive to the probability of false alarm in the range of 10^{-4} to 10^{-8}, with the higher false-alarm rates giving slightly lower losses.

The summary gives an example of a radar design to illustrate the use of the present results.

14. SUBJECT TERMS		15. NUMBER OF PAGES
radar loses	eclipsing loss	60
electrically scanned array	beam straddle loss	16. PRICE CODE
search patterns	radar scanning optimization	

17. SECURITY CLASSIFICATION OF REPORT	18. SECURITY CLASSIFICATION OF THIS PAGE	19. SECURITY CLASSIFICATION OF ABSTRACT	20. LIMITATION OF ABSTRACT
Unclassified	Unclassified	Unclassified	

MASSACHUSETTS INSTITUTE OF TECHNOLOGY
LINCOLN LABORATORY

BEAM AND FILTER STRADDLE LOSSES IN AN ESA SEARCH RADAR

R.J. GALEJS
C.E. MUEHE
Group 411

TECHNICAL REPORT 947

31 MARCH 1992

Approved for public release; distribution is unlimited.

LEXINGTON MASSACHUSETTS

ABSTRACT

The present study was undertaken to quantify several types of losses encountered when using an electronically-scanned array (ESA). The losses examined include beam straddle losses, eclipsing losses, and range-Doppler straddling losses. The losses were studied for volume search radars with square and hexagonal search patterns as well as horizon search radar.

The radar search equations for an ESA radar for both volume and horizon search are first derived. The beam straddle loss is then found, including the effect of range eclipsing for a high pulse repetition frequency (PRF) radar. The hexagonal search pattern has about 0.5 to 1 dB less loss than the square search. This loss is a strong function of probability of detection and duty factor precluding the insertion of a constant loss term in the radar range equation for these effects. A derivation of range and Doppler straddling losses follows, showing that they vary only slightly with the probability of detection and thus can be represented by a constant depending only on range-gate and Doppler-filter spacings. All losses were found to be very insensitive to the probability of false alarm in the range of 10^{-4} to 10^{-8}, with the higher false-alarm rates giving slightly lower losses.

The summary gives an example of a radar design to illustrate the use of the present results.

DTIC COPY INSPECTED

Accession For
NTIS GRA&I
DTIC TAB
Unannounced
Justification
By
Distribution/
Availability Codes
Dist | Avail and/or Special
A-1

TABLE OF CONTENTS

LIST OF ILLUSTRATIONS

LIST OF TABLES

1. INTRODUCTION

The beam straddle, eclipsing, and filter straddle losses for radars employing electronically scanned antennas (ESAs) when operating in the search mode are derived in this report. An ESA is a passive or an active phased array. A passive ESA has a phase shifter at each element, whereas an active array has a transmit/receive module at each element. In either case, the ESA is step scanned in space. This contrasts with a mechanically scanned antenna that sweeps past a target in a continuous motion. A proper account of the difference in scanning between ESA and mechanically scanned radars in the search mode complicates the detection performance of ESA radars. Mechanically scanned fan-beam radars have a 1.6-dB single-scan loss when noncoherent integration is employed and a 1.7-dB loss with coherent integration, practically independent of probability of detection [1]. The single-scan loss for ESA radars is a function of the probability of detection, the spacing and geometrical positioning of the beams and, for a high pulse repetition frequency (PRF) radar, the duty cycle of the waveform employed. While the loss for a mechanically scanned radar is easily calculated as a reduction in the received signal energy from its peak value due to the changing antenna gain as it sweeps past the target, the performance loss of an ESA radar must be judged from the average probability of detection with an assumed target distribution in range, angle, and Doppler space. In this report, the target is assumed to have a uniform distribution in angle (azimuth and elevation), range, and Doppler.

There is relatively little literature about beam straddle losses for an ESA [2,3,4]. In Evans, Hahn, and Hank, the loss is correctly found using statistical averaging (probability of detection averaging rather than power averaging) but only four beams are considered when calculating the losses for a volume search. This is much too low for the case of highly overlapping beams. In this report, 37 beams are used to ensure that the detection probability from all relevant beams is accounted for. None of the papers start from a radar range equation so that it is difficult to discern the meaning of the calculated losses from a radar design point of view. The hexagonal search pattern was found to be slightly better than the square search pattern [3,4]. The present work shows the hexagonal search to be 0.5 to 1 dB better. Eclipsing and range-Doppler straddle losses are also computed as well as beam straddle for horizon scan.

The radar search equations for an ESA radar for both volume and horizon search are first derived. The beam straddle loss is then found, including the effect of range eclipsing for a high PRF radar. This loss is a strong function of probability of detection and duty factor precluding the insertion of a constant loss term in the radar range equation for these effects. A derivation of range and Doppler straddling losses follows, showing that they vary only slightly with the probability of detection and thus can be represented by a constant depending only on range-gate and Doppler-filter spacings. All losses were found to be very insensitive to the probability of false alarm in the range from 10^{-4} to 10^{-8} with the higher false-alarm rates giving slightly lower losses.

2. RADAR EQUATION FOR SEARCH

The search form of the radar range equation for both horizon and volume search is derived in this section. The derivation includes the efficiency and antenna beam broadening factors that affect overall search performance. A more refined version of the radar search equation than is usually given in textbooks is required when evaluating search pattern losses.

The power received from a target is

$$P_r = \frac{P_t G_t}{4\pi R^2} \frac{\sigma_t}{4\pi R^2} A_r. \tag{1}$$

This expression is divided into three parts. The first part is the power density (W/m^2) at a target a distance R away and at the peak of the antenna beam. P_t is the power radiated from the antenna and G_t is the transmit antenna gain. The target, with radar cross section σ_t, is assumed to capture and isotropically reradiate all the energy incident upon that cross section so that the power density back at the receiver is the product of the first two terms. The receiving antenna has an effective receiving area, A_r, given by its actual area, A, oriented to intercept the maximum reflected energy multiplied by an efficiency factor, η_r. If the receive area is an array, η_r is determined by the type of weighting employed to reduce antenna sidelobes. For a uniform weighting, $\eta_r = 1$. Tables for various weightings along with beam broadening coefficients can be found in Barton and Ward [5].

The received signal must compete with receiver noise for detection to occur. The receiver noise is kT_0F_nB where k is the Boltzmann constant, T_0 is the standard reference temperature such that $kT_0 = 4 \times 10^{-21}$ J, F_n is the radar system noise figure, and B is the noise bandwidth of the receiver. If coherent processing using a weighted matched filter is employed, the noise bandwidth is a constant times the reciprocal of the coherent integration time τ. This constant can be found in Barton and Ward [5] for various weightings. This analysis will include this constant as well as other departures from the ideal in a loss term L to arrive at the first form of the search equation,

$$\frac{S}{N} = \frac{P_{av}\tau G_t A \eta_r \sigma_t}{(4\pi)^2 R^4 k T_0 F_n L}. \tag{2}$$

The transmit antenna gain is $4\pi A\eta_t/\lambda^2$, so that Equation (2) becomes

$$\frac{S}{N} = \frac{P_{av}\tau A^2 \sigma_t \eta_t \eta_r}{4\pi R^4 k T_0 F_n L \lambda^2}. \tag{3}$$

Up to this point no distinction has been made between volume and horizon search. From this point on, two sets of equations will be derived, one for volume search and one for horizon search.

When an electronically scanned antenna searches a solid angle, the beam successively points to a large number of beam positions in either a rectangular or hexagonal pattern. The spacing of the beam and the dwell time, τ, per beam position are adjusted so that the solid angle coverage will occur in the scan time T_s. To analyze the performance, the two-way antenna gain function,

$$G_2 = G_{20} \exp\left(-(4\ln 2)\left[\frac{1}{\theta_{3tx}^2} + \frac{1}{\theta_{3rx}^2}\right]\theta_x^2\right) \exp\left(-(4\ln 2)\left[\frac{1}{\theta_{3ty}^2} + \frac{1}{\theta_{3ry}^2}\right]\theta_y^2\right) \tag{4}$$

must be introduced. For horizon search, the search pattern is one dimensional so that a given angle will be covered in the scan time. For this case, a one-dimensional pattern is required that is given by

$$G_{2h} = G_{20h} \exp\left(-(4\ln 2)\left[\frac{1}{\theta_{3tx}^2} + \frac{1}{\theta_{3rx}^2}\right]\theta_x^2\right). \tag{5}$$

In Equation (4) the antenna beam is modeled as a two-dimensional Gaussian with a peak two-way gain of G_{20}. A more realistic beam shape such as a sinc pattern has a negligible effect on the loss results (see Appendix B). For either an elliptical or rectangular antenna, the one-way beam shape is elliptical with major and minor axes in the orthogonal x and y directions. In Equation (5) the antenna beam is a one-dimensional Gaussian with a peak two-way gain of G_{20h}. The 3-dB beamwidths are expressed as

$$\theta_{3tx} = \frac{k_{tx}\lambda}{D_x} \tag{6}$$

$$\theta_{3ty} = \frac{k_{ty}\lambda}{D_y} \tag{7}$$

$$\theta_{3rx} = \frac{k_{rx}\lambda}{D_x} \tag{8}$$

$$\theta_{3ry} = \frac{k_{ry}\lambda}{D_y}, \tag{9}$$

where λ is the wavelength, D_x and D_y are the dimensions of the antenna, and the k's are the beam broadening factors produced by the various antenna weightings employed (see Barton and Ward [5]). The subscripts r and t refer to the receive and transmit beams respectively. Only Equations (6) and (8) are relevant for horizon search. The reader is cautioned that Barton and Ward [5] provides two types of k's. The first is for a linear antenna and would apply to each dimension of a rectangular antenna. The second set of k's applies to circular or elliptical antennas that are weighted radially and in which case $k_{tx} = k_{ty}$ and $k_{rx} = k_{ry}$.

In the analyses of beam scanning performance it is convenient to normalize the spacing of the beams to the 3-dB one-way beamwidths θ_{3x} and θ_{3y} (or equivalently the 6-dB two-way beamwidths). These are given by

$$\frac{2}{\theta_{3x}^2} = \frac{1}{\theta_{3tx}^2} + \frac{1}{\theta_{3rx}^2}, \tag{10}$$

$$\frac{2}{\theta_{3y}^2} = \frac{1}{\theta_{3ty}^2} + \frac{1}{\theta_{3ry}^2}. \tag{11}$$

Substituting Equations (10) and (11) into Equation (4) yields

$$G_2 = G_{20} \exp\left(-(8 \ln 2)\left[\frac{\theta_x^2}{\theta_{3x}^2} + \frac{\theta_y^2}{\theta_{3y}^2}\right]\right) \tag{12}$$

for volume search and substituting Equation (10) into Equation (5) yields

$$G_{2h} = G_{20h} \exp\left(-(8 \ln 2)\frac{\theta_x^2}{\theta_{3x}^2}\right) \tag{13}$$

for horizon search.

The beam spacing is defined in terms of the 3-dB one-way beamwidths so that the solid angle searched by one beam position can be written

$$\psi = \theta_{1x}\theta_{1y} = \alpha_x \alpha_y \theta_{3x}\theta_{3y} \tag{14}$$

where α_x is the spacing to beamwidth ratio in the x direction, α_y in the y direction [see Figures 1(a) and 1(b)]. For a uniform hexagonal search pattern with circular beams, $\theta_{3x} = \theta_{3y}$ and $\alpha_y = \alpha_x\sqrt{3}/2$. The angle searched in the horizon search can be written

$$\psi_h = \theta_1 = \alpha\theta_3 \tag{15}$$

[see Figure 1(c)]. The constants α are related to the gain of the beams at the overlap point. This relationship is given in Table 1 for the values of α used in the plots.

The integration time τ in the radar range equation [Equation (3)] will be replaced by noting that the total search solid angle Ω can be searched in T_s seconds if it takes τ seconds to search one beam position of solid angle ψ. Using Equation (14),

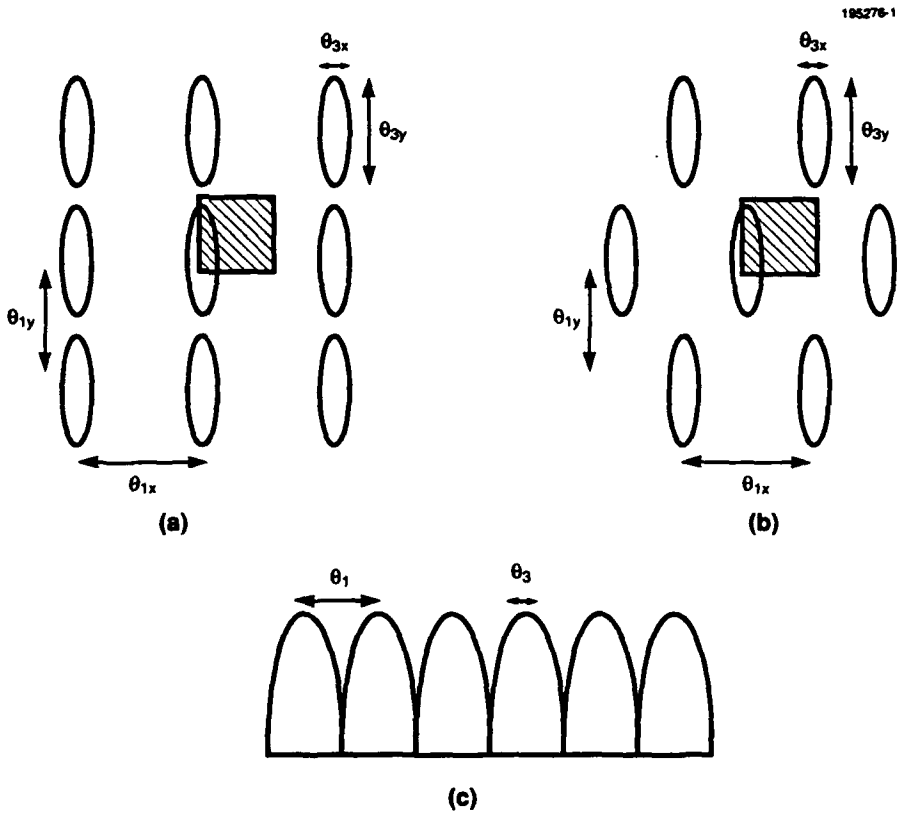

Figure 1. Beam spacing geometry: (a) square search, (b) hexagonal search, and (c) horizon search.

TABLE 1

Antenna Gains at Overlap Point with Adjacent Beams

α	dB
0.5	-.75
0.7	-1.5
1.0	-3.0
1.4	-5.9
2.0	-12.0

$$\tau = \frac{T_s \psi}{\Omega} = \frac{T_s \alpha_x \alpha_y \theta_{3x} \theta_{3y}}{\Omega}. \tag{16}$$

For horizon search the angle Ω_h can be searched in T_s seconds if it takes τ_h seconds to search one beam position of angle ψ_h. Using Equation (15),

$$\tau_h = \frac{T_s \psi_h}{\Omega_h} = \frac{T_s \alpha \theta_3}{\Omega_h}. \tag{17}$$

Substituting Equation (16) into Equation (3) yields

$$\frac{S}{N} = \frac{P_{av} A \sigma_t T_s \eta_t \eta_r \alpha_x \alpha_y}{4\pi R^4 k T_0 F_n L \Omega} \frac{\theta_{3x} \theta_{3y} A}{\lambda^2} \tag{18}$$

for volume search. Substituting Equation (17) into Equation (3) yields

$$\frac{S}{N} = \frac{P_{av} A \sigma_t T_s \eta_t \eta_r \alpha D_y}{4\pi R^4 k T_0 F_n L \Omega_h \lambda} \frac{\theta_3 D_x}{\lambda} \tag{19}$$

for horizon search.

Using Equations (6) to (11), the last term in Equation (18) may be written

$$\frac{\theta_{3x} \theta_{3y} A}{\lambda^2} = \frac{2K_2}{(1/k_{tx}^2 + 1/k_{rx}^2)^{1/2} (1/k_{ty}^2 + 1/k_{ry}^2)^{1/2}}, \tag{20}$$

where K_2 accounts for the relation between antenna dimensions and area so that $K_2 = \pi/4$ for an elliptical antenna and $K_2 = 1$ for a rectangular antenna. For horizon search, Equations (6), (8), and (10) can be combined to rewrite the last term in Equation (19) as

$$\frac{\theta_{3x} D_x}{\lambda} = \left[\frac{2}{1/k_{tx}^2 + 1/k_{rx}^2} \right]^{1/2}. \tag{21}$$

The final form of the radar range equation for volume search is found by substituting Equation (20) into Equation (18) giving

$$\frac{S}{N} = \frac{P_{av} A \sigma_t T_s}{4\pi R^4 k T_0 F_n L \Omega} \frac{1}{L_w} \alpha_x \alpha_y \tag{22}$$

where

$$L_w = \frac{(1/k_{tx}^2 + 1/k_{rx}^2)^{1/2}(1/k_{ty}^2 + 1/k_{ry}^2)^{1/2}}{2K_2\eta_t\eta_r}. \tag{23}$$

The final form of the radar range equation for horizon search is found by substituting Equation (21) into Equation (19) giving

$$\frac{S}{N} = \frac{P_{av}AD_y\sigma_t T_s}{4\pi R^4 kT_0 F_n L\Omega_h \lambda}\frac{1}{L_{wh}}\alpha_x \tag{24}$$

where

$$L_{wh} = \frac{(1/k_{tx}^2 + 1/k_{rx}^2)^{1/2}}{2^{1/2}\eta_t\eta_r}. \tag{25}$$

Equations (22) and (24) have been divided into three terms. The first term results from a simplified analysis in which the antenna efficiencies and beam spreading factors are ignored. The second term introduces an antenna weighting loss term, Equation (23) or Equation (25), that includes the effects of these factors. The third term accounts for the variation in the signal-to-noise ratio (SNR) due to beam spacing.

The loss term L in Equations (22) and (24) has been included to account for departures from the ideal. It is assumed that a common reference point is chosen to measure the average transmitted power, P_{av}, and the system noise figure, F_n. It is suggested that the face of the antenna just outside of the radome be taken as the reference. If this point is chosen, then the microwave and radome transmit loss will be included in P_{av}, and the receive loss including radome loss will be included in the system noise figure F_n.

All other losses will be included in the loss term L. These may include: range and Doppler filter efficiency loss, constant false-alarm rate (CFAR) loss, quantization loss, propagation loss, clutter fill loss, and off-boresite scan loss.

Table 2 presents the weighting losses (L_w and L_{wh}), beam broadening factors (k), and antenna efficiencies (η), for circular, square, and fan beam antennas in which the transmit weighting is uniform and the receive weighting utilizes various Taylor weightings. For uniform illumination, $k = 0.885$ for linear weighting and 1.106 for circular weighting with $\eta = 1$ for both.

TABLE 2

Taylor Weighting Losses, Beam Broadening Factors, and Antenna Efficiencies for a Given Sidelobe Level Below the Peak of the Main Beam

Sidelobe Level (dB)	L_w (dB)			k		η	
	Circular Antenna	Square Antenna	Fan Beam	Circular	Linear	Circular	Linear
20	0.82	1.06	.53	1.076	.983	.966	.951
25	0.90	1.29	.65	1.120	1.049	.914	.900
30	1.09	1.58	.79	1.164	1.115	.846	.850
35	1.26	1.88	.94	1.234	1.179	.774	.804
40	1.52	2.16	1.08	1.287	1.250	.706	.763
45	1.75	2.48	1.24	1.334	1.301	.651	.726

3. BEAM SCAN AND ECLIPSING

3.1 Averaged Probability of Detection

Appendix A derives the probability of detection as a function of the signal-to-noise ratio (SNR) and the probability of false alarms for a constant, nonfluctuating target and a Swerling I target. The probability of nondetection is more convenient to use in this analysis and is given by Equation (A.7) and Equation (A.12) for the constant and Swerling I targets respectively. These probabilities are cumulated over all beams with significant detection probability, averaged over all possible target positions, and subtracted from unity to give the true detection probability.

First, the volume search probabilities are derived. A square search pattern is assumed, with the azimuth beams spaced by an angle θ_{1x} and the elevation beams spaced by an angle θ_{1y}. The azimuth and elevation beamwidths are θ_{3x} and θ_{3y} respectively [see Figure 1(a)]. The central beam and the 37 surrounding beams are considered [see Figure 2(a)]. An examination of the antenna gains shows that any beams further away will have a negligible effect on the results for the range of α values used here. If smaller α values are considered then more beams need to be included. These beams are formed at different times (at possibly different frequencies) so that the target returns may be considered independent with target fluctuations from one beam to another. Thus, the Swerling I result will be used to model the probability of nondetection. The total probability of nondetection over the beams is the product of Equation (A.12) for all of the beams. This probability is then averaged over a representative sample of azimuth-elevation space [see shaded rectangle in Figure 1(a)] assuming that the target position is uniformly distributed over angles. The total probability of detection is 1 minus the averaged product of nondetection. This may be written

$$P_d = 1 - 4\int_0^{1/2}\int_0^{1/2}\prod_{i=1}^{37}(1 - P_{FA}^{1/(1+\rho_i)})dxdy. \tag{26}$$

In this equation, the angles have been normalized by the beam separation, $x = \theta_{AZ}/\theta_{1x}$, $y = \theta_{EL}/\theta_{1y}$, and i designates one of the 37 beams. The SNR, ρ_i, will vary according to the separation of the search beams and the location of a target relative to a beam peak.

The SNR in Equation (22) must be modified to account for the two-way antenna gain, Equation (12). Assuming the beams are Gaussian yields,

$$\rho_i = \rho_0\alpha_x\alpha_y \exp(-(8\ln 2)[\alpha_x^2(x - x(i))^2 + \alpha_y^2(y - y(i))^2]), \tag{27}$$

where

$$\rho_0 = \frac{P_{av}A\sigma_t T_s}{4\pi R^4 k T_0 F_n \Omega L L_w}. \tag{28}$$

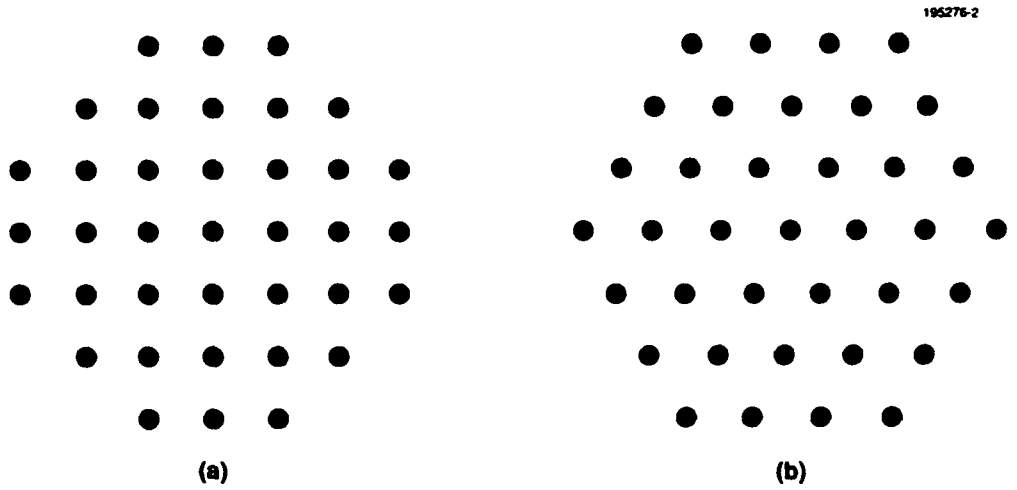

Figure 2. Beam positions used in loss calculation for (a) square search and (b) hexagonal search.

The above results do not include the effects of eclipsing. Eclipsing occurs because the receiver cannot be turned on during transmission. A schematic of the transmit/receive cycle is given in Figure 3. The duty cycle, D_u, indicates what fraction of a pulse repetition interval (PRI) the transmission is on. Thus, if the PRI has a length of 1, then the transmission has a length D_u. The received signal is processed with a matched filter of length D_u. When this filter does not overlap the transmit pulse, then the full SNR is realized. However, some of the time this filter does overlap the transmit pulse. Then the SNR falls quadratically according to what fraction of the transmit pulse and matched filter are overlapped (see Figure 3). With overlap, the voltage out of the filter varies linearly with the overlap so that the signal power varies as the overlap squared while the noise remains constant. Thus, for a time $1 - 2\ D_u$, the full SNR is realized, and for a time $2\ D_u$, the SNR varies quadratically with time. The detection probability is now

$$P_d = 1 - (1 - 2D_u)4 \int_0^{1/2} \int_0^{1/2} \prod_{i=1}^{37} (1 - P_{FA}^{1/(1+\rho_i)}) d\tau$$

$$-2D_u 4 \int_0^1 \int_0^{1/2} \int_0^{1/2} \prod_{i=1}^{37} (1 - P_{FA}^{1/(1+t^2\rho_i)}) dx dy dt, \tag{29}$$

where ρ_i is given by Equation (27). The t integral represents the integral over the $2\ D_u$ interval of reduced SNR.

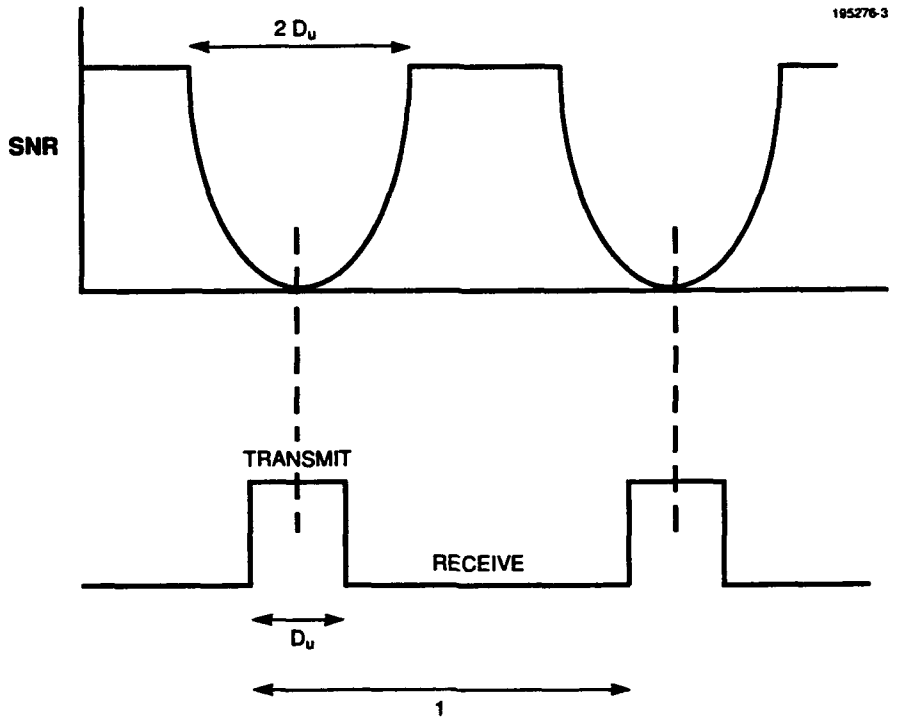

Figure 3. Reduced SNR due to eclipsing.

The equations for the hexagonal search pattern are identical to the square search equations just presented, except for a different definition of the $x(i)$ and $y(i)$. See Figure 2(b) for the beam locations in hexagonal search.

The eclipsing loss may also be derived by itself, assuming that the target is always at the peak of the radar beam. For this case, the detection probability may be written

$$P_d = 1 - (1 - 2D_u)(1 - P_{FA}^{1/(1+\rho)}) - 2D_u \int_0^1 (1 - P_{FA}^{1/(1+t^2\rho)})dt. \tag{30}$$

The horizon search probabilities are now derived. In this case, 11 beams are considered: the central beam and the ten adjacent beams. A Swerling I target is also assumed. The total probability of nondetection over the beams is the product of Equation (A.12) for the 11 beams. This probability is then averaged over a representative sample of angles. The total probability of detection is 1 minus the averaged product of nondetection. This may be written as

$$P_d = 1 - 2\int_0^{1/2} \prod_{i=-5}^{5} (1 - P_{FA}^{1/(1+\rho_i)})dx. \tag{31}$$

In this equation, the angle has been normalized by the beam separation, $x = \theta_{AZ}/\theta_{1x}$ and i designates one of the 11 beams. The SNR, ρ_i, will vary depending on the separation of the search beams and the location of a target relative to a beam peak.

The SNR in Equation (24) must be modified to account for the two-way antenna gain Equation (13). Assuming the beams are Gaussian yields,

$$\rho_i = \rho_{0h}\alpha_x \exp(-(8\ln 2)\alpha_x^2(x-i)^2), \tag{32}$$

where

$$\rho_{0h} = \frac{P_{av}AD_y\sigma_t T_s}{4\pi R^4 k T_0 F_n \lambda \Omega_h L L_w}. \tag{33}$$

Eclipsing is accounted for in the same manner as for volume search. The detection probability is now

$$\begin{aligned} P_d &= 1-(1-2D_u)2\int_0^{1/2}\prod_{i=-5}^{5}(1-P_{FA}^{1/(1+\rho_h)})dx \\ &\quad -2D_u 2\int_0^1\int_0^{1/2}\prod_{i=-5}^{5}(1-P_{FA}^{1/(1+t^2\rho_h)})dxdt, \end{aligned} \tag{34}$$

where ρ_i is given by Equation (32).

3.2 Results

The probability of detection (P_d) curves vs SNR for hexagonal scan are plotted in Figures 4(a-d) for duty factors of 0, 0.1, 0.2, and 0.3 respectively. On each curve the dashed line represents the result of a Swerling I target at the peak of a single beam with $\alpha_x\alpha_y = 1$, which is used as a reference. The probability of false alarm was taken as 10^{-6}. Five values for α are shown: 0.5, 0.7, 1, 1.4, and 2, each indicated by a different symbol. For this hexagonal case, $\alpha_x = \alpha$ and $\alpha_y = \alpha\sqrt{3}/2$.

The zero duty factor case (as if there were no eclipsing)[Figure 4(a)] shows that for low SNR and hence low P_d, widely spaced beams (large α) provide the optimum search scheme while at large SNR and large P_d, closely spaced overlapping beams (small α) provide the best search scheme. At intermediate P_d, the usual 3-dB overlap ($\alpha = 1$) is optimum. At high P_d there is the somewhat surprising gain over the reference case. This gain results from the contribution to the overall P_d from the many beams averaged over a representative sample of azimuth-elevation space compared to the P_d from the peak of a single beam with $\alpha_x\alpha_y = 1$. The contribution from the surrounding beams is quite significant at the higher SNRs.

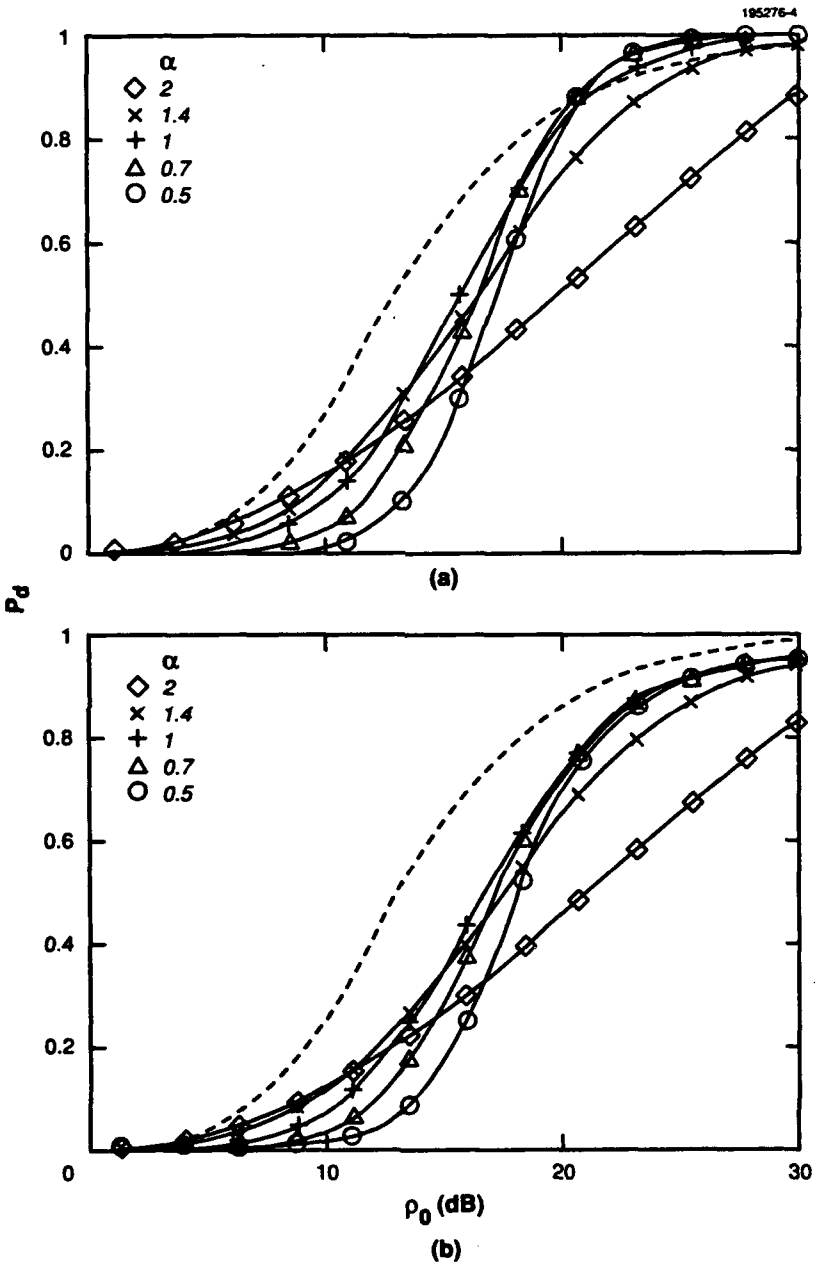

Figure 4. Probability of detection for hexagonal search pattern with $P_{fa} = 10^{-6}$. *(a)* $D_u = 0$ *and (b)* $D_u = 0.1$.

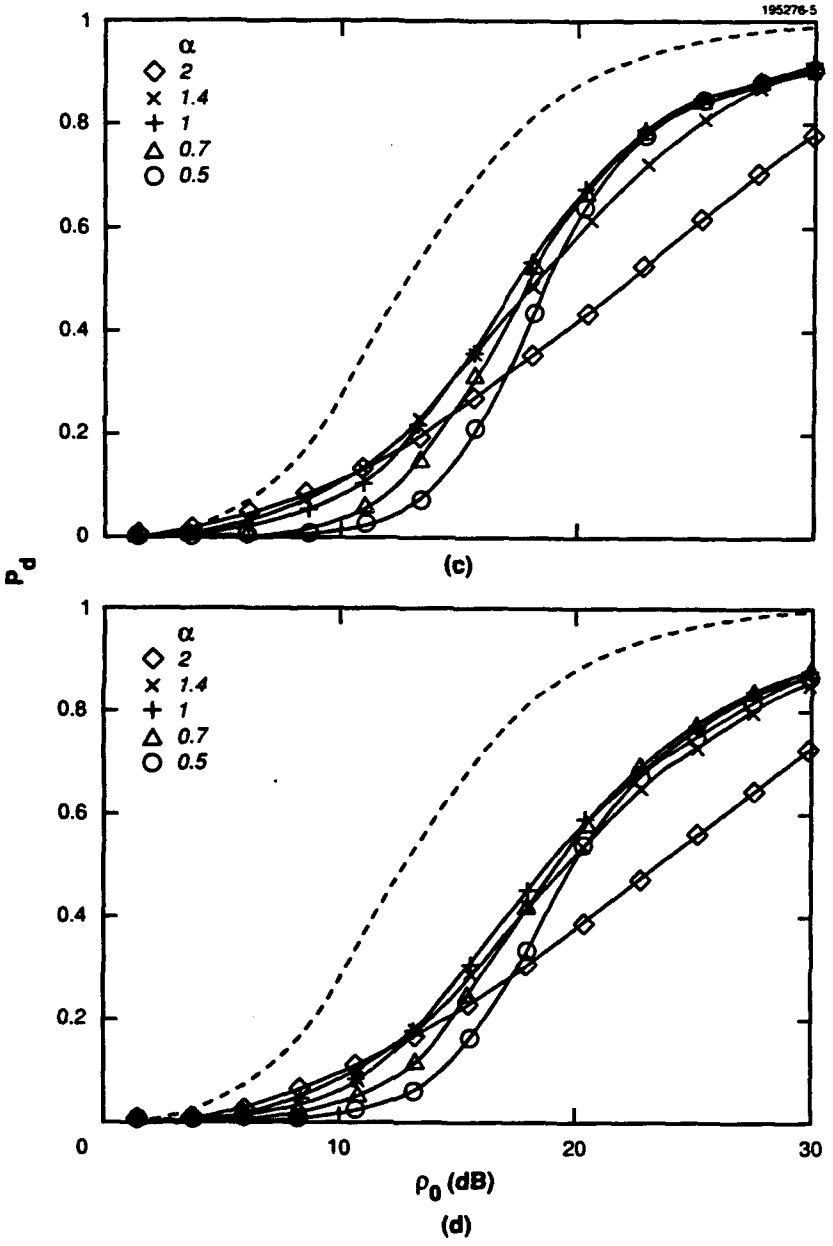

Figure 4. Probability of detection for hexagonal search pattern with $P_{fa} = 10^{-6}$. *(c)* $D_u = 0.2$ *and (d)* $D_u = 0.3$.

As the duty factor increases [Figures 4(b-d)], there appears a significant loss at a higher P_d. The best case search scheme at 30-dB SNR achieves only a 0.95 P_d for D_u =0.1, 0.9 P_d at 0.2 D_u, and 0.85 P_d at 0.3 D_u, compared with the nearly 1 P_d at D_u=0. In addition, at higher P_d the trend of increasing performance with decreasing α no longer holds. At D_u=0.1 and 0.2, the optimum α at the highest P_d shown is 0.7 while at D_u = 0.3, α = 1 remains optimum from about P_d=0.2 on up.

The effect of the differing search schemes for hexagonal scan becomes more obvious in Figures 5(a-d), which show the increase in SNR necessary to achieve the same P_d as the Swerling I reference (the definition of loss). The optimum scan pattern and corresponding loss is easily found for each case by looking at the lower bound of the different curves. This better illustrates the differences discussed in the previous paragraph. In general, the loss is a strong function of P_d even for constant α. This prevents the insertion of a constant loss term in the radar range equation to account for beam straddle losses. Each P_d must be considered separately.

The square search pattern results are very similar to the hexagonal search case but a little worse in terms of losses. Figures 6(a-d) show the additional loss over the hexagonal search for D_u=0, 0.1, 0.2, and 0.3 respectively, for the same range of α as before. In general, the square search pattern does about 0.5 to 1 dB worse. To see this, compare Figures 5(a) and 6(a). From P_d = 0 to about 0.15, α = 2 is the optimum hexagonal scan choice with the square scan giving 0 to 1 dB of additional loss; for P_d=0.15 to 0.3, α =1.4 is the best with 0.5 to 1 dB of additional loss; for P_d=0.3 to 0.7, α =1.0 is the best with 0.5 to 0.75 dB of additional loss; for P_d=0.7 to 0.9, α =0.7 is the best with 0.5 to 1 dB of additional loss, and finally for P_d=0.9 to 1, α=0.5 is best with $\sim$1 dB more loss. The square scan gives a slightly different optimum α vs P_d, but the envelope is always about 0.5 to 1 dB worse than hexagonal scan.

Two other P_{fa} were investigated: 10^{-4} and 10^{-8}. The $P_{fa} = 10^{-8}$ losses for both hexagonal and square scans over all duty factors were virtually indistinguishable from the 10^{-6} results with the differences being less than 0.1 dB. The $P_{fa} = 10^{-4}$ losses were slightly less than for 10^{-6} but only by about 0.1 to 0.25 dB. Due to this close similarity no plots for other P_{fa} are included here.

The choice of α for a given radar design depends on the requirements of that radar. If a single-hit P_d of 0.5 is required, then α = 1 is the best choice. For higher single hit P_d, smaller values of α are optimum, but α = 1 is at most 1 dB from optimum for P_d=0.3 on up. If a radar is designed around cumulative detection, which would operate in the lower single hit P_d range, a larger α with bigger beam spacing would be the best for the constant frame time assumed here. Thus, the optimum volume search design depends on the actual radar requirements but, in general, the standard choice α = 1 does fairly well, if not optimally.

The horizon search results are presented in Figures 7 and 8, with 7(a-d) showing P_d vs SNR and 8(a-d) showing loss vs P_d. These results show many of the same features as the volume search case. For low P_d, large α is best and at high P_d, low α is best. In general, the losses are less, due to the one-dimensional nature of the problem, and the low α cases are optimum over a broader range

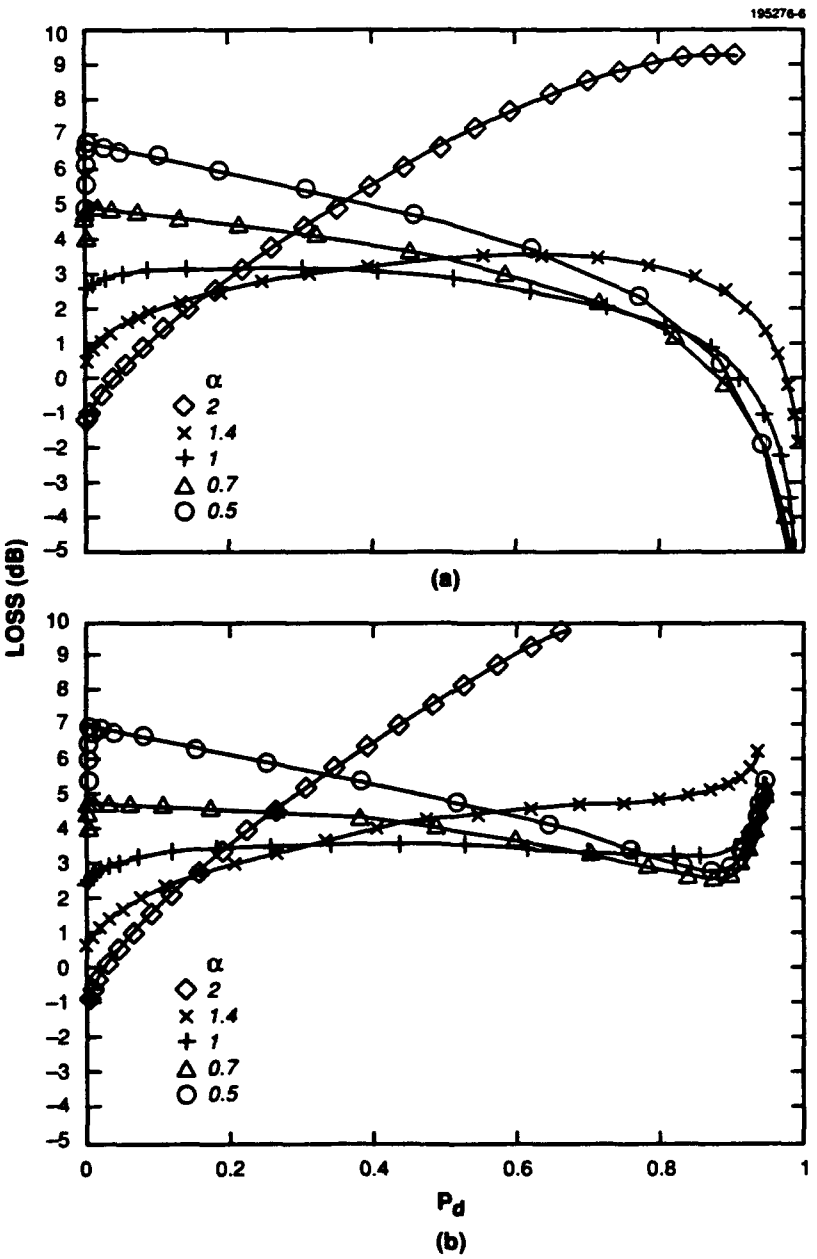

Figure 5. Losses for hexagonal search pattern with $P_{fa} = 10^{-6}$. *(a)* $D_u = 0$ *and (b)* $D_u = 0.1$.

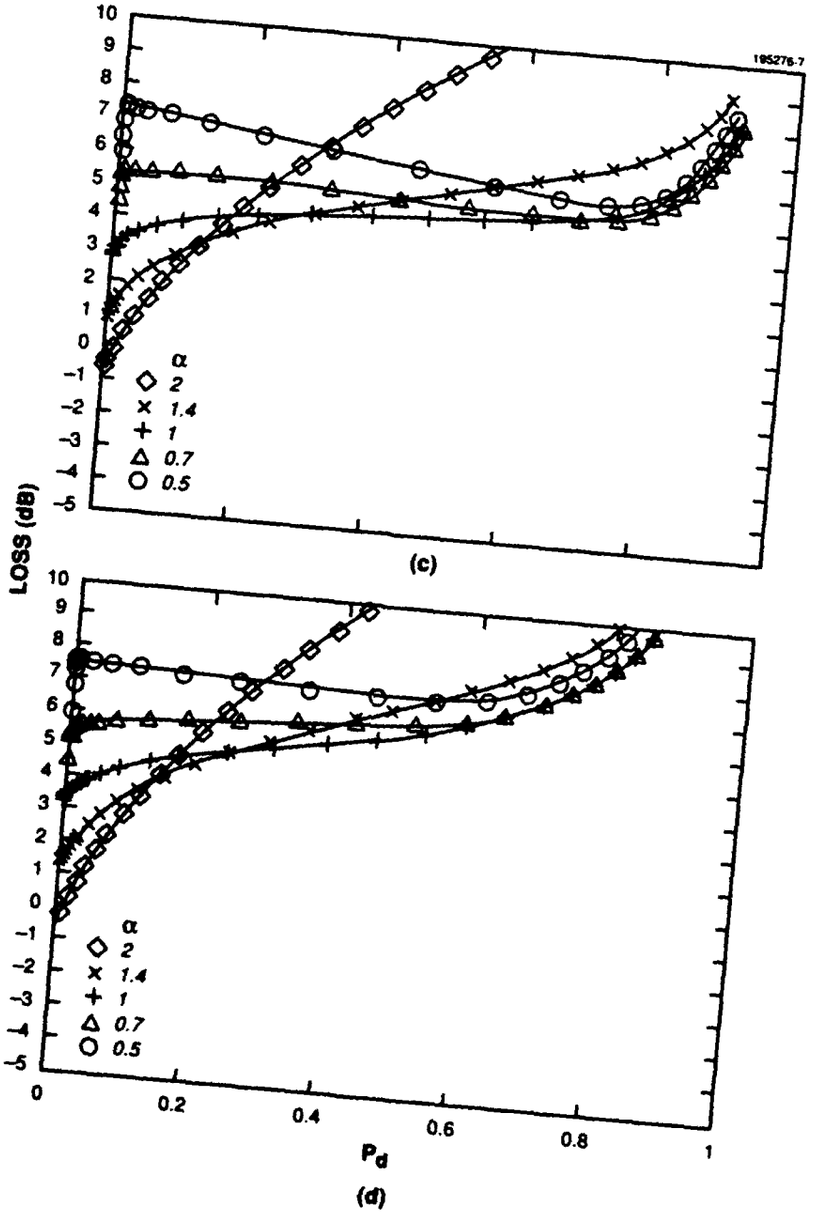

Figure 5. Losses for hexagonal search pattern with $P_{fa} = 10^{-6}$. (c) $D_u = 0.2$ and (d) $D_u = 0.3$.

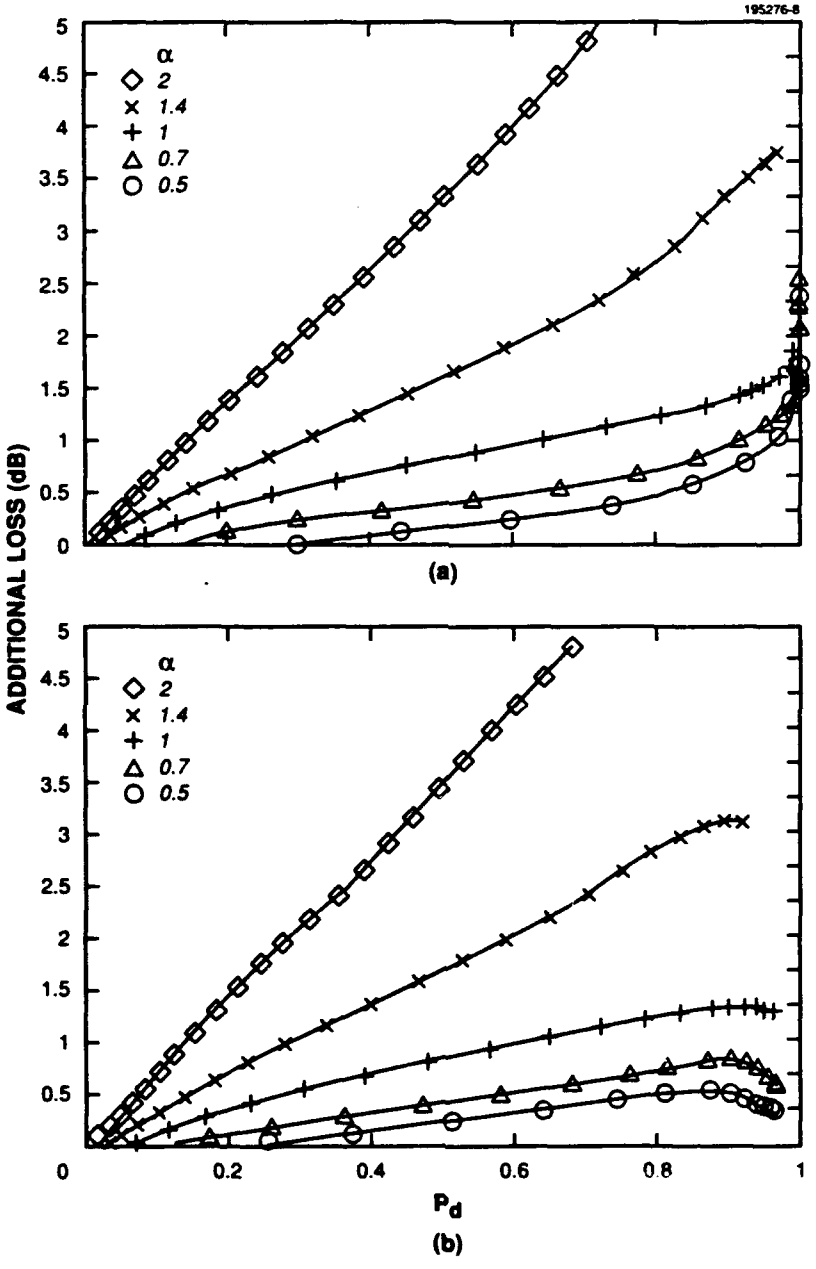

Figure 6. Additional losses for square search pattern with $P_{fa} = 10^{-6}$. (a) $D_u = 0$ and (b) $D_u = 0.1$.

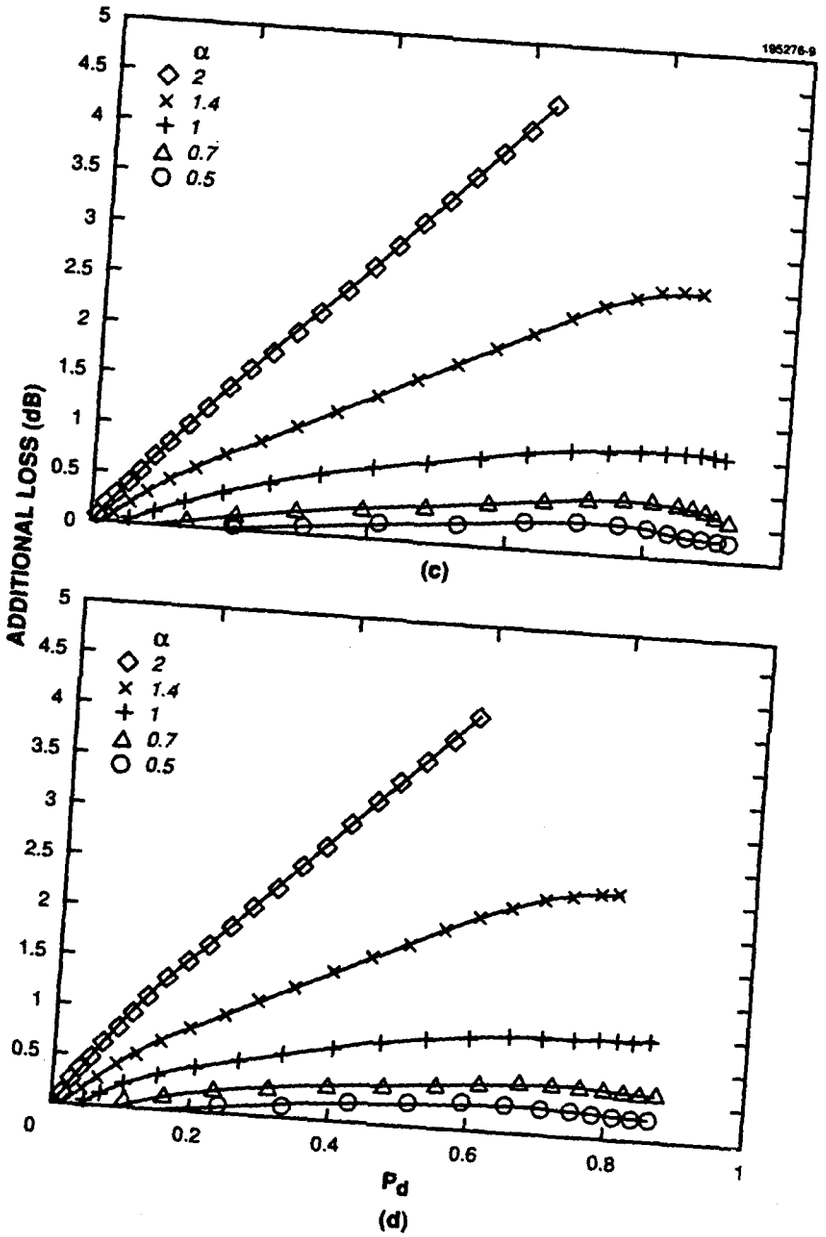

Figure 6. Additional losses for square search pattern with $P_{fa} = 10^{-6}$. (c) $D_u = 0.2$ and (d) $D_u = 0.3$.

of P_d at the expense of the α=1 case. Also, the low α case remains optimum even at large duty factors.

Overall, the design criteria for a horizon search radar are similar to those for volume search. However, smaller α with more overlap between beams is favored. In this case, α=0.7 appears to be the best overall choice for horizon search.

The effect of eclipsing alone is shown in Figures 9 and 10. The P_d vs SNR is shown in Figure 9 for D_u=0.1, 0.2, 0.3, and 0.4 and the corresponding losses in Figure 10. The losses are not constant with P_d and thus cannot be included in the radar range equation as a constant loss factor. In addition, eclipsing and beam straddle losses are not additive. This can be seen by comparing Figures 5(a) and 5(d). If the losses were additive then the relative losses between α would not change with varying D_u. However, in Figure 5(a) (D_u=0), the crossing point for α = 2 and α = 0.5 occurs at P_d=0.35, while in Figure 5(d) (D_u=0.3), the crossing point occurs at P_d=0.25. Thus, the losses shown in Figure 10 give a fair indication of the magnitude of the eclipsing losses, but for an accurate calculation, both beam straddle and eclipsing losses must be considered together.

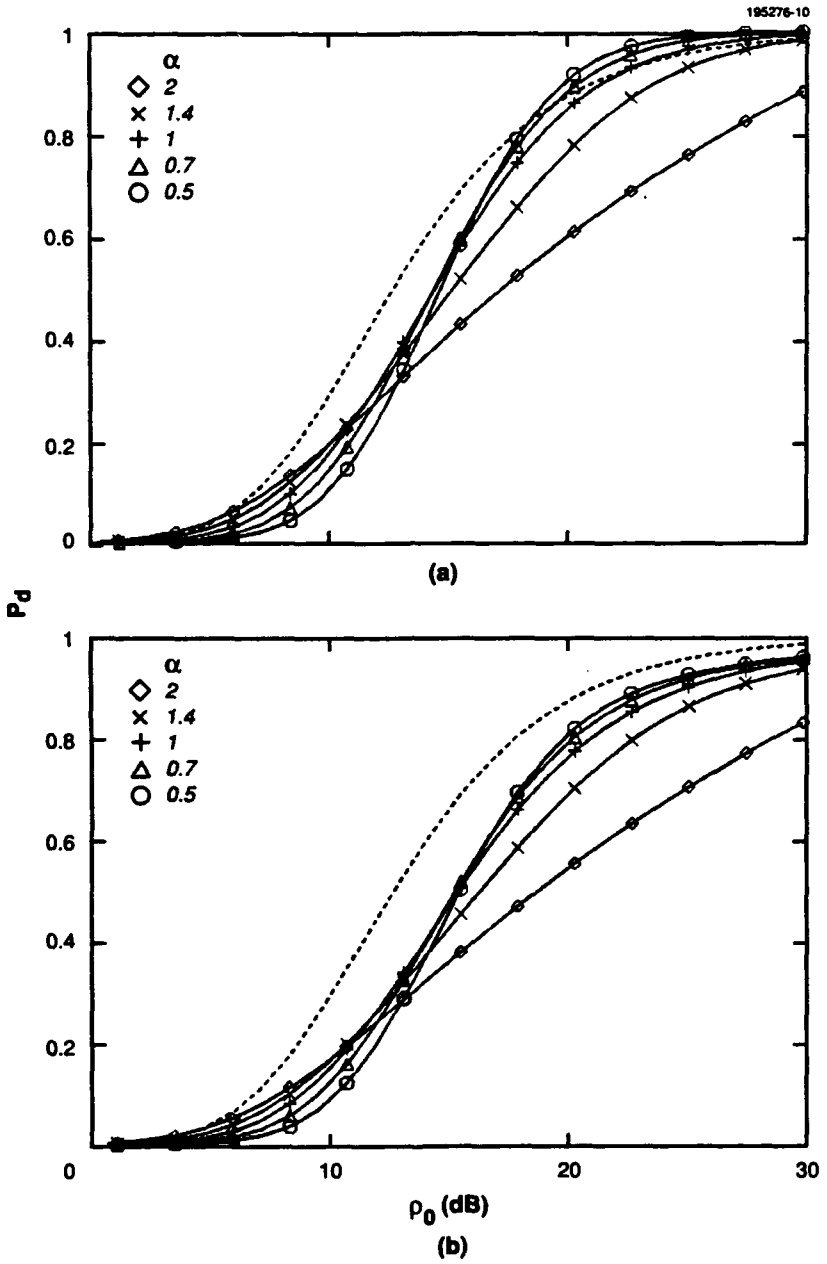

Figure 7. Probability of detection for horizon search with $P_{fa} = 10^{-6}$. *(a)* $D_u = 0$ *and (b)* $D_u = 0.1$.

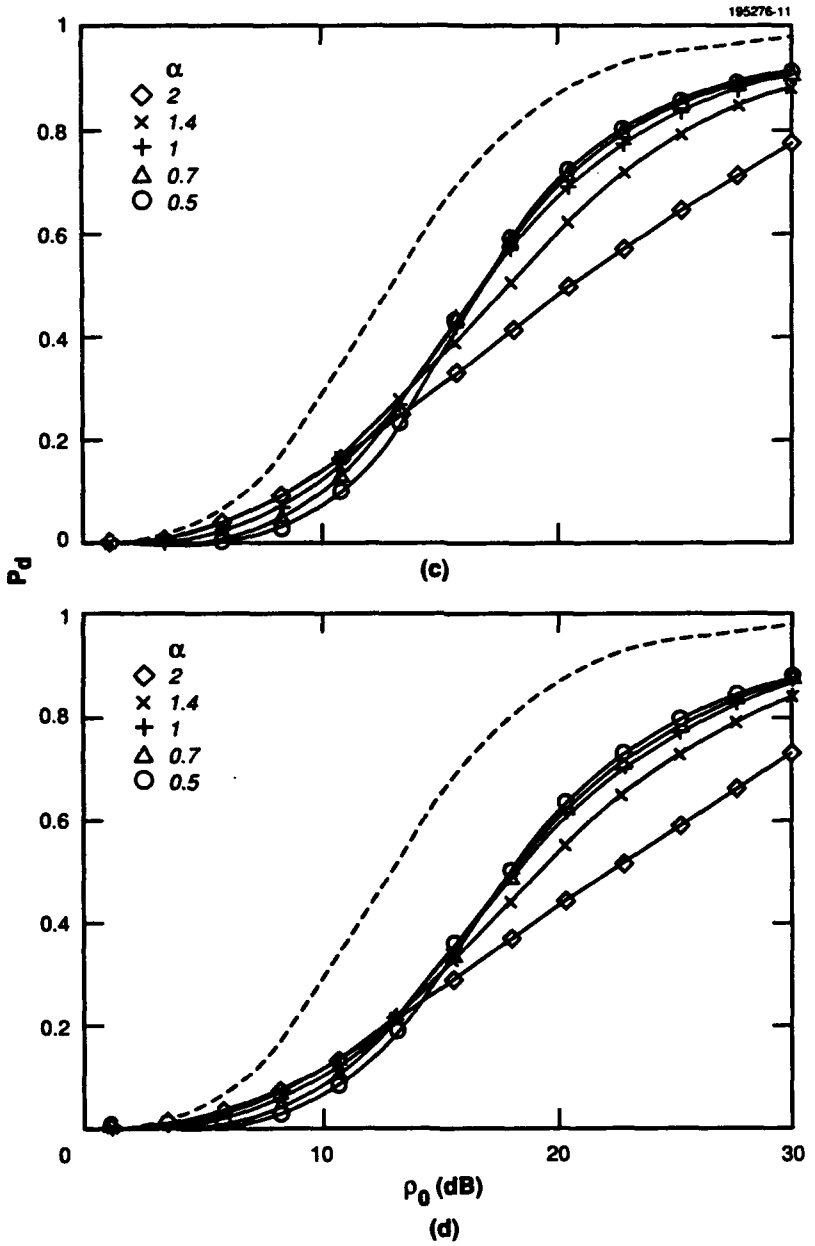

Figure 7. Probability of detection for horizon search with $P_{fa} = 10^{-6}$. (c) $D_u = 0.2$ and (d) $D_u = 0.3$.

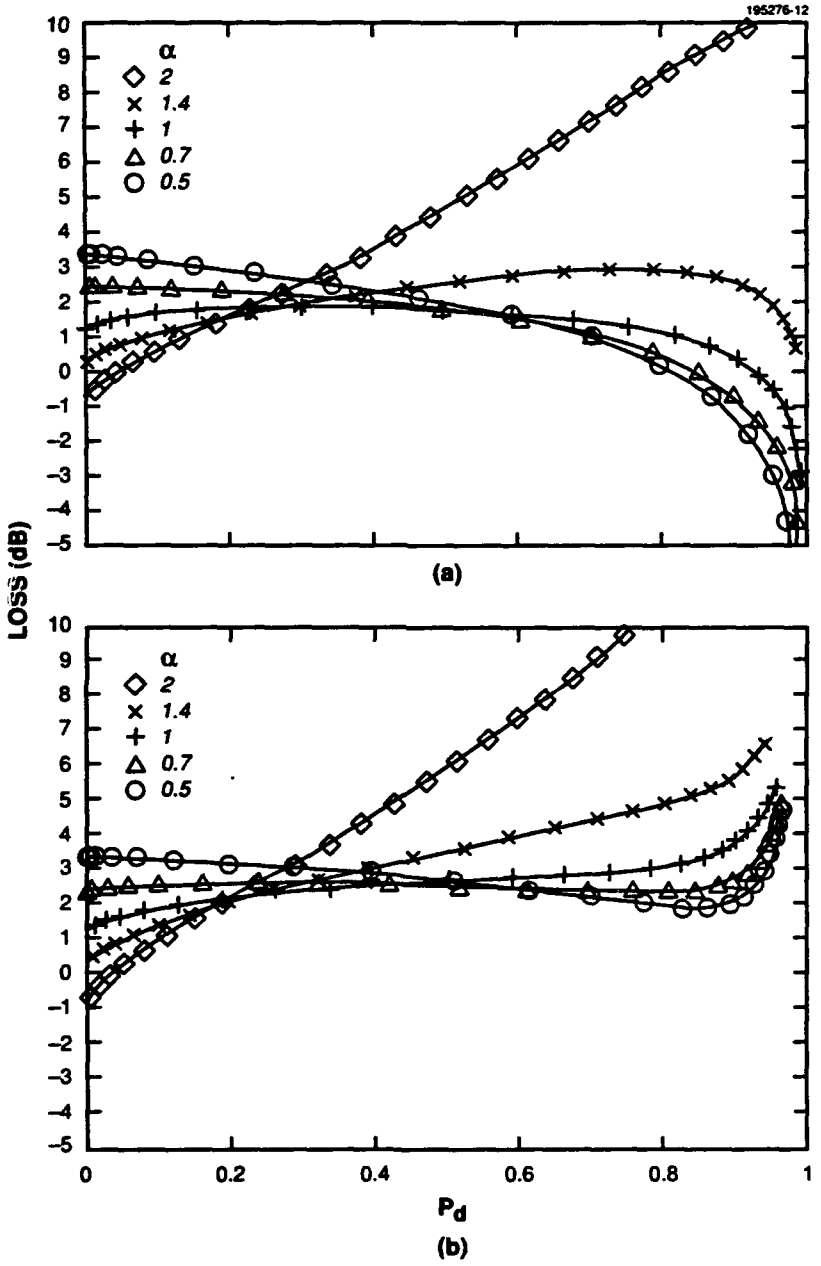

Figure 8. Losses for horizon search with $P_{fa} = 10^{-6}$. (a) $D_u = 0$ and (b) $D_u = 0.1$.

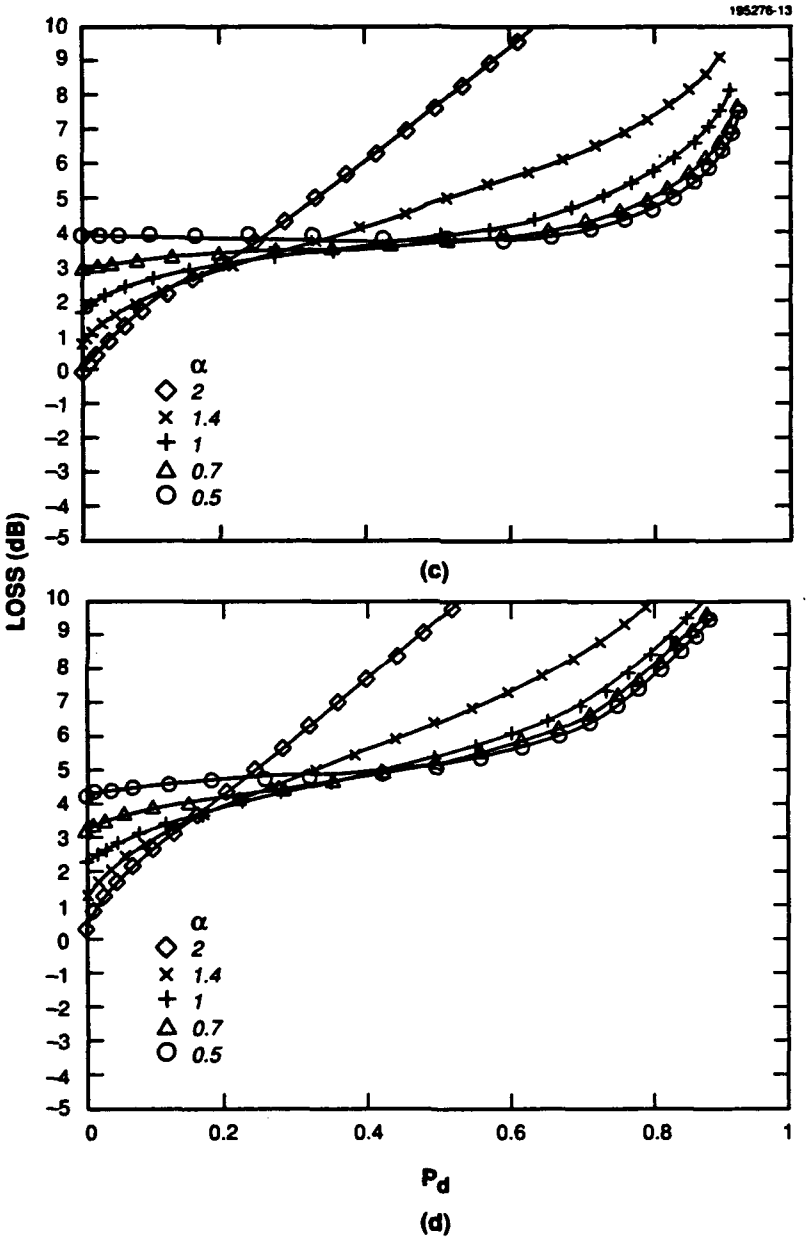

Figure 8. Losses for horizon search with $P_{fa} = 10^{-6}$. (c) $D_u = 0.2$ and (d) $D_u = 0.3$.

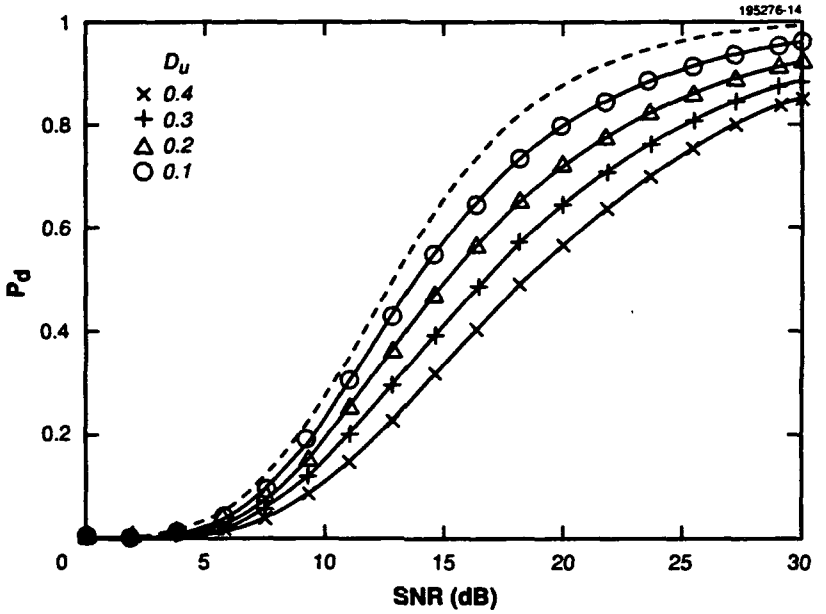

Figure 9. Effect of eclipsing on probability of detection with $P_{fa} = 10^{-6}$.

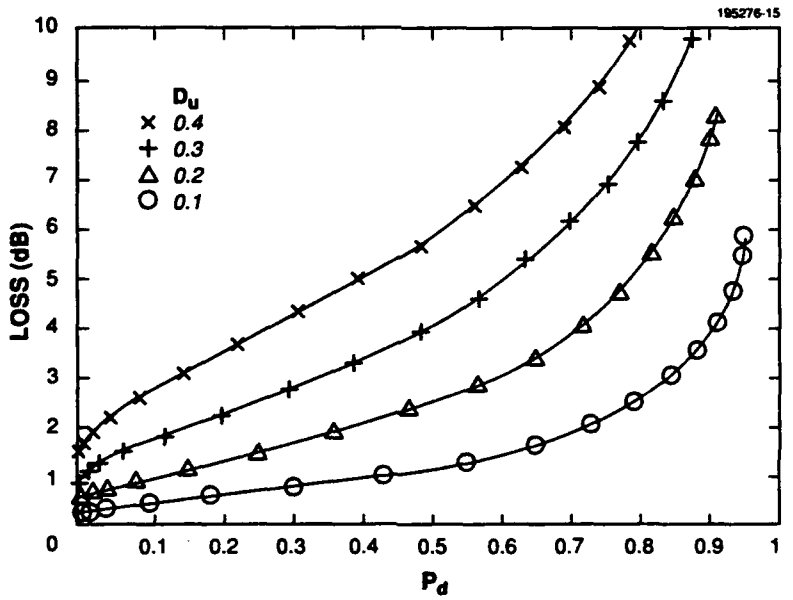

Figure 10. Eclipsing losses with $P_{fa} = 10^{-6}$. *Target is at beam center.*

4. RANGE-DOPPLER STRADDLING

4.1 Averaged Probability of Detection

In range-Doppler space, the probability of detection is calculated similarly to beam straddle loss. However, in this case, the target does not fluctuate from filter to filter because all of the range-Doppler cells under consideration are formed at the same time. Thus, Q_C from Equation (A.7) will be used for the probability of nondetection. After the averaged probability of nondetection is found, this probability must then be averaged over the SNR distribution because the SNR will vary from one scan to the next. If the noise is assumed to be uncorrelated from filter to filter, then the following is the probability of detection for a given filter and the eight surrounding filters:

$$P_d = 1 - \frac{4}{\rho}\int_0^\infty \int_0^{1/2}\int_0^{1/2} \prod_{k=-1}^{1}\prod_{l=-1}^{1} Q_C(\rho_{kl})dzdw\exp(-\rho_1/\rho)d\rho_1, \tag{35}$$

where

$$\rho_{kl} = \rho_1 \exp[-(4\ln 2)\alpha_w^2(w-l)^2 - (4\ln 2)\alpha_z^2(z-k)^2], \tag{36}$$

$\alpha_w = r_1/r_3$, $\alpha_z = d_1/d_3$, $w = r/r_1$, and $z = d/d_1$. r and d refer to distances in the range and Doppler dimensions respectively, the subscript 1 refers to the spacing of the filters and the subscript 3 to the 3 dB width of the filters. Adding more filters did not significantly change the results. The P_d calculated in Equation (35) is optimistic because the noise from cell to cell is actually correlated. The cells overlap and correspond to the same time samples. Thus, the assumption of independent looks at the target from each range-Doppler cell is incorrect. This P_d is an upper bound on the true P_d.

In order to treat the correlated noise properly, the joint nondetection probability must be treated differently from the product of the Q_C functions used in Equation (35). For the case of correlated noise, the probability density function of the nine complex signals is [7]

$$P(\vec{Z}) = \frac{1}{\sqrt{(2\pi)^N\Delta}}\exp\left[-\frac{1}{2}(\vec{S}-\vec{Z})^\dagger\bar{\bar{R}}^{-1}(\vec{S}-\vec{Z})\right], \tag{37}$$

where $\vec{S}$ is the 18-vector (nine real and nine imaginary components) of the ideal signal, $\vec{Z}$ the 18-vector of the measured signal plus noise, $\bar{\bar{R}}$ the covariance matrix between the noise components of $\vec{Z}$, Δ the determinant of $\bar{\bar{R}}$, and $N = 18$. The probability of nondetection would be

$$P_{nd} = \int_{A_1=0}^{b} \int_{A_2=0}^{b} \cdots \int_{A_N=0}^{b} P(\vec{A}) A_1 A_2 \cdots A_N d\vec{A}, \tag{38}$$

where

$$P(\vec{A}) = \int P(\vec{Z}) d\vec{\phi}. \tag{39}$$

$\vec{\phi}$ indicates all the phases of $\vec{Z}$. This process is illustrated for a single set of I and Q channels with uncorrelated noise (see Appendix A).

This procedure turns out to be a formidable task with its 18-dimensional integrals and matrix inversions and was not investigated further. Instead, a lower bound on the P_d was found by averaging over the central range-Doppler cell alone [Equation (35) with $k = l = 0$ only]. In this case, the integral over ρ_1 may be performed first to yield

$$P_d = 1 - 4 \int_0^{1/2} \int_0^{1/2} (1 - P_{FA}^{1/(1+\rho)}) dz dw \tag{40}$$

where

$$\rho = \rho_0 \exp(-(4 \ln 2)\alpha_w^2 w^2 - (4 \ln 2)\alpha_z^2 z^2). \tag{41}$$

Thus, two bounds were found: a lower bound from Equation (40) and an upper bound from Equation (35). In certain cases, the upper bound may actually yield a gain when there should always be a loss. A stricter upper bound would then be the lesser of 0 dB or Equation (35).

4.2 Results

The probability of detection curves vs SNR for range-Doppler straddling are plotted in Figure 11 for $\alpha_z = \alpha_w = 0.7$, 1, 1.4, and 2. The solid curves show the upper bound on the P_d given by Equation (35) and the dashed curve the lower bound [Equation(40)]. The dot-dash line gives the Swerling I result as a reference. The α=0.5 case is not shown because it always falls within a small fraction of a decibel of the reference. The shaded regions between the lines show the range in which the true P_d lies. In all cases, the uncertainty is less than a decibel.

The loss vs P_d curves are plotted in Figure 12. The loss is defined as before as the increase in SNR required to achieve the same P_d as the Swerling I case. The losses are plotted with the solid line giving the lower bound on the loss, the dashed line the upper bound, with the shaded area between showing the range in which the true loss lies. As α increases, the two bounds approach one another, putting very tight limits on the loss that is quite high. At lower α with greater beam overlap, the loss is low with a large uncertainty. Lower α (≤ 1) is of the most interest. At these

low values, the loss is essentially constant with P_d so that the range-Doppler straddling loss may be included in the loss term of the radar range equation as a constant.

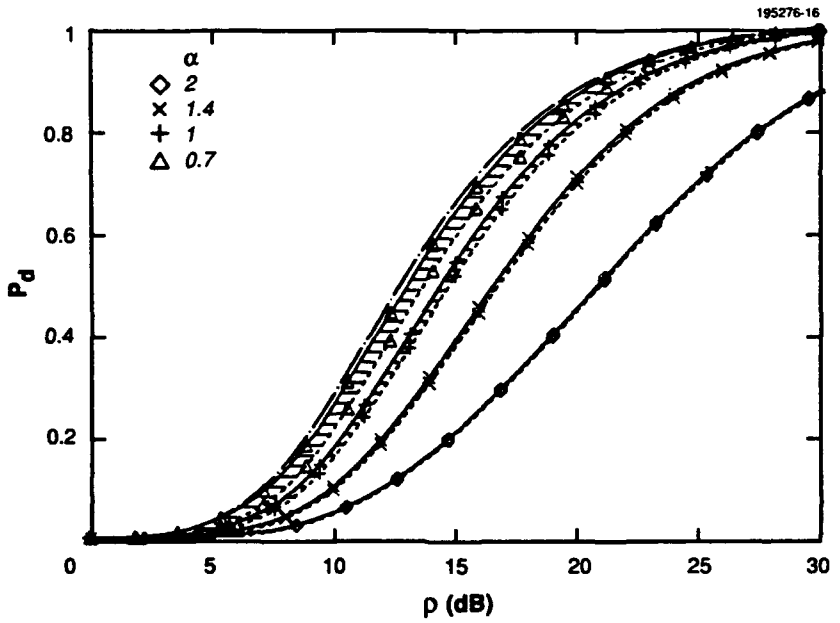

Figure 11. Probability of detection with range-Doppler straddling.

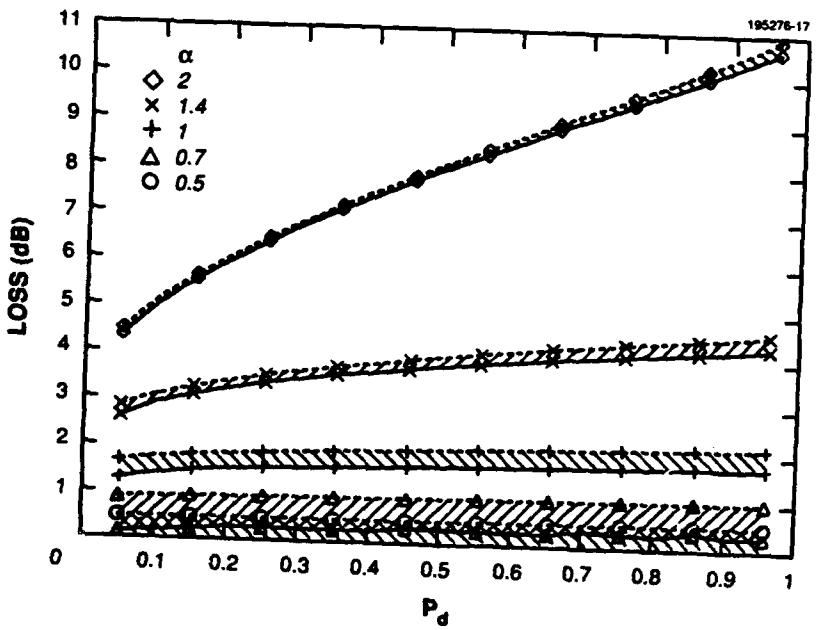

Figure 12. Range-Doppler straddling loss.

5. CONCLUSIONS

5.1 Summary

Many modern radars, by utilizing an ESA, can perform a variety of functions including volume search and dedicated target tracking. Volume search usually occupies the largest fraction of an ESA radar's time and resources. Thus, to prevent over- or under-design, an accurate prediction of its performance in the search mode is highly desired.

Accurate versions of the radar range equation for two-dimensional volume search and horizon search were derived. These equations involve loss terms that often depend on the desired probability of detection, P_d, such as the antenna scanning loss (pattern loss) and range eclipsing loss. Loss terms that are essentially independent of P_d are the range-Doppler straddling and weighting losses, to reduce the antenna sidelobes or the range-Doppler sidelobes.

The derivation of the antenna scanning and eclipsing losses assumes a Swerling I target and either a hexagonal or square grid of antenna beam positions in space or uniformly spaced fan beams on the horizon. Detection is assumed to be statistically independent from beam to beam, and a cumulative detection probability over all nearby beams is calculated. The target's position is assumed to be distributed evenly in angle and range because the actual target location is unknown. Thus, the detection probability is found by averaging over all angles and ranges.

The loss results for hexagonal and square search patterns are shown in Figures 5 and 6 and for horizon search in Figure 8. Eclipsing loss alone is shown in Figure 10. A comparison of Figure 10 with Figures 5, 6, and 8 shows that eclipsing loss cannot simply be added to the scanning loss to find the total. Rather, the combined effects of beam scan and eclipsing must be considered together.

Range-Doppler straddling loss is shown in Figure 12. This figure shows that for reasonably spaced cells ($\alpha \leq 1$) the sum of the range and Doppler straddle loss is less than 2 dB and nearly independent of P_d. Thus, the range-Doppler straddling loss may be added as a constant to the radar range equation.

5.2 Loss Reduction

There are many ways in which losses could be reduced below the levels calculated earlier. In general, these methods achieve only a modest decrease in loss at the expense of much greater processing requirements and/or more complicated hardware. Three methods will be discussed briefly in this section: multiple receive beams, staggered beam positions from scan to scan, and staggered PRFs.

Multiple receive beams require multiple receive channels in the radar. This involves both more radar hardware and signal processing. In this scheme, several highly overlapping receive beams are processed instead of a single beam. Figure 13 shows a case in which there are five receive beams

instead of the usual one. This is similar to using closely spaced sequential beams that minimize the SNR loss from the peak of the beam. However, for multiple receive beams, the different channels are not independent so that the loss calculation requires methods similar to the range-Doppler straddle loss where loss bounds may be found. The best performance using multiple receive beams can be calculated by assuming that the target is always at the peak of a receive beam, thus neglecting the SNR loss from the receive beam not pointing directly at a target. Similar reduction in range-Doppler straddle loss may be achieved by using many closely spaced filters, increasing the signal processing load immensely.

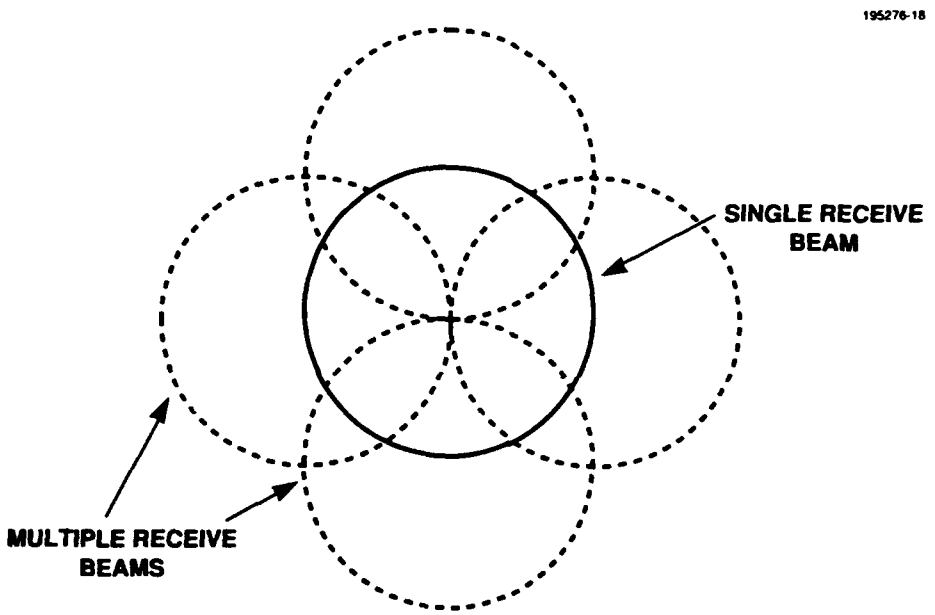

Figure 13. Multiple receive beams.

Staggered beam positions are used to "fill in" the gaps between beams on a previous scan. Figure 14 illustrates such a search scheme. If a target happened to fall at the center of four beams in a square search pattern, then on the next scan the target would be at the peak of beam. This only reduces losses if the performance is calculated on a best-of-two scan basis. The definition of losses would have to be modified for this case because a constant frame time was assumed in this study and the effective frame time for this method would be doubled. Otherwise, this beam shifting would tend to average the target over all possible beam positions, as was done in the calculations.

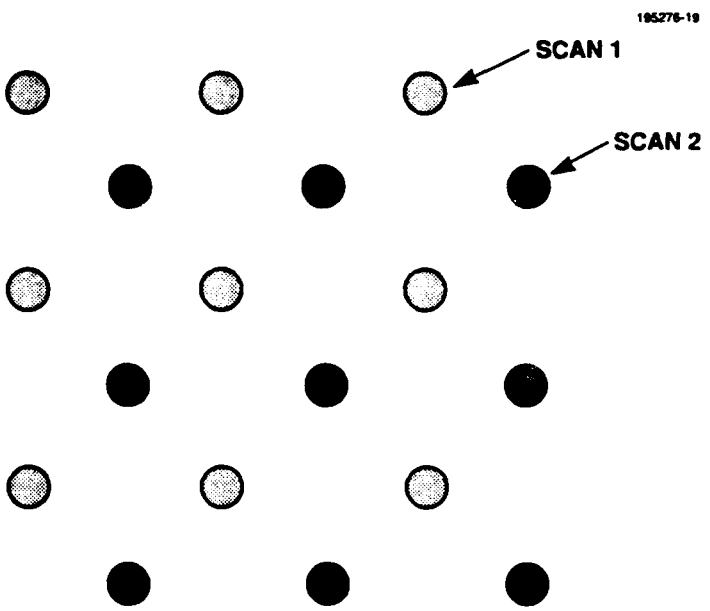

Figure 14. Staggered beam positions.

Staggered PRFs are similar to the staggered beam positions except now the eclipsing losses are affected. Figure 15 shows the varying eclipsed regions from two PRFs. Once again, if losses are calculated on a best-of-two basis then they may be reduced after accounting for the increased frame time. Otherwise, the PRF shifts would average the target over all possible locations with respect to the transmitted pulse.

5.3 Example Loss Calculation

As an example, consider a typical ESA radar. A P_d of 0.5 is specified with $P_{fa} = 10^{-6}$. The antenna is circular and is unweighted on transmit but weighted with -40-dB sidelobes on receive to reduce ECM effects. From Table 2 the weighting loss is 1.52 dB. To reduce the effect of large targets or clutter, the range and Doppler sidelobes are set at -30 dB below the peak. This results in a 0.79-dB (see Table 2) loss in each dimension. The range-Doppler cells will be spaced equal to their 3-dB response points ($\alpha = 1$) so as not to overburden the signal processor. Figure 10 shows the resulting loss to be 1.75 dB at $P_d = 0.5$. A duty cycle of 0.2 is chosen for the radar and a hexagonal antenna search pattern is to be employed. From Figure 5(c), the best choice of $\alpha = 1$ is chosen for $P_d = 0.5$, resulting in a combined scanning and straddling loss of 4.5 dB. These radar design parameters and the corresponding losses are shown in Table 3.

TABLE 3

Parameters and Losses for a Typical ESA Radar

Parameter	
Antenna Shape	Circular
Transmit Sidelobes	Unweighted
Receive Sidelobe	-40 dB
Range Sidelobes	-30 dB
Doppler Sidelobes	-30 dB
Range-Doppler Cell Overlap Point	-3 dB
Scan Pattern	Hexagonal
Beam Overlap Point	-3 dB
P_d	0.5
P_{fa}	10^{-6}
Duty Cycle	0.2
Losses	
Antenna Weighting	1.52 dB
Antenna Scanning and Eclipsing	4.5 dB
Range Weighting	.79 dB
Doppler Weighting	.79 dB
Range-Doppler Straddling	1.75 dB
Total	9.35 dB

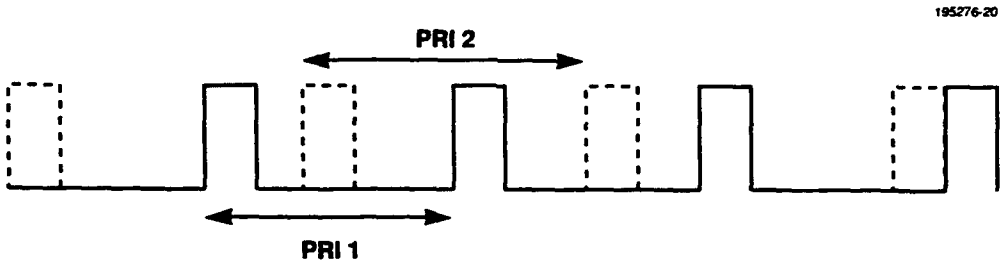

Figure 15. Staggered PRFs.

The total loss shown is 9.35 dB. Several other losses must be included in the radar range equation. They include but are not limited to CFAR loss from the limited accuracy available to estimate the adaptive thresholds, quantization loss caused by the addition of quantization noise from the limited number of bits in the A/D converters, propagation loss, clutter-fill loss from the transmission of pulses that are not integrated but are used to correlate the clutter return, and off-boresite scanning loss from the loss in gain as the ESA scans away from the boresite.

Of the 9.35-dB loss about half (4.5 dB) is from the antenna scanning plus range eclipsing. From Figure 5(a), this loss could be reduced to 2.7 dB if the eclipsing were eliminated by going to a much smaller duty factor or using separate transmit and receive antennas.

Some of the losses derived in this report apply to radars used for target tracking using either a mechanically scanned antenna or an ESA. These include eclipsing losses and range-Doppler straddle losses. If adaptive PRFs and Doppler filtering are employed then these losses may be reduced by centering the filter of interest on the predicted location of the target in track.

For an ESA in the search mode, it may be more appropriate to specify the cumulative detection probability of a target as it approaches the radar over a period of time. This may be accomplished either through an alert-confirm process or a simple cumulative detection scheme. In alert-confirm, once a detection at a relatively large P_{fa} has been made, it is confirmed with a longer dwell following

quickly after the initial detection. In the cumulative detection process a given search pattern is followed with no change made after a given detection. The analysis of cumulative detection requires the addition of another variable, the search frame time in which the desired volume is scanned. This will be the subject of another report.

APPENDIX A
PROBABILITY OF DETECTION

The joint probability density function for the two components of a complex signal embedded in Gaussian noise of variance N_0 is

$$P(I,Q) = \frac{1}{2\pi N_0} \exp\left(-\frac{(I-I_0)^2 + (Q-Q_0)^2}{2N_0}\right), \tag{A.1}$$

where I and Q are the in-phase and quadrature components of the signal plus noise and I_0 and Q_0 are the corresponding components of the signal alone. Detection occurs when the amplitude of the complex signal plus noise exceeds a threshold b. This threshold is determined by the desired false-alarm rate. The probability of detection may be written

$$P_d = \int\int_{I^2+Q^2>b^2} P(I,Q)dIdQ \tag{A.2}$$

or, equivalently in polar coordinates

$$P_d = \int_{A=b}^{\infty}\int_{\theta=0}^{2\pi} P(A,\theta)AdAd\theta, \tag{A.3}$$

where

$$P(A,\theta) = \frac{1}{2\pi N_0} \exp\left(-\frac{(A\cos\theta - A_0\cos\theta_0)^2 + (A\sin\theta - A_0\sin\theta_0)^2}{2N_0}\right). \tag{A.4}$$

The integral over θ in Equation(A.3) may be performed to yield

$$P_d = \int_{A=b}^{\infty} \frac{A}{N_0} \exp\left(-\frac{A^2+A_0^2}{2N_0}\right) I_0\left(\frac{AA_0}{N_0}\right) dA, \tag{A.5}$$

where I_0 is the modified Bessel function of the first kind. This integrand is a Rician density function. Equation (A.5) may be written in terms of the SNR, ρ, by letting $\rho = A_0^2/(2N_0)$ and $u = A^2/(2N_0)$. Then, the integral becomes

$$P_d = \int_{u=b'}^{\infty} \exp(-\rho - u) I_0(2\sqrt{\rho u}) du. \tag{A.6}$$

The threshold is found by letting the SNR $\rho = 0$ in Equation (A.6), which then becomes the expression for P_{fa}, the probability of false alarm. The threshold to satisfy a given false-alarm probability is $b' = -\ln P_{fa}$.

The probability of nondetection is of more interest in this study and may be written

$$Q_C(\rho) = 1 - P_d = \int_{u=0}^{-\ln P_{FA}} \exp(-\rho - u) I_0(2\sqrt{\rho u}) du. \tag{A.7}$$

The subscript C indicates that this result is for a constant, nonfluctuating target. A handy approximation for Q_C was found:

$$Q_C(\rho) \sim \exp\left[-\left(\frac{\rho}{B}\right)^a\right]. \tag{A.8}$$

This analytical form was found to be a good approximation to $Q_C(\rho)$ for $0 < \rho < 30$, the region of most interest. This form also allows much more rapid numerical evaluation of Equation (35), an approximation in itself, which would otherwise be a triple integral over a product of nine integrals. Table A-1 shows the values of a and B to use in this approximation for several P_{fa} values.

TABLE A-1

Parameters for Q Function Approximation

P_{fa}	a	B
10^{-4}	2.31	10.3
10^{-6}	2.86	15.3
10^{-8}	3.35	20.6

For the case of a fluctuating target, there is a different probability of nondetection, Q_F, which is Q_C averaged over the probability density of the SNR.

$$Q_F(\rho) = 1/\rho \int_0^\infty Q_C(\rho_1) \exp(-\rho_1/\rho) d\rho_1. \tag{A.9}$$

A Swerling I type target exhibits this type of exponential target fluctuation. Substituting Equation (A.7) for Q_C and reversing the order of integration yields

$$Q_F(\rho) = 1/\rho \int_0^{-\ln P_{FA}} \exp(-u) \int_0^{\infty} \exp(-\rho_1(1 + 1/\rho)) I_0(2\sqrt{u\rho_1}) d\rho_1 du. \qquad \text{(A.10)}$$

The integral over ρ_1 may be accomplished with the help of Equations 6.614, 9.220, and 9.215 of Abromowitz and Stegun [6]. These yield the simple result

$$Q_F(\rho) = 1/(\rho + 1) \int_0^{-\ln P_{FA}} \exp(-u(1/(1 + \rho)) du. \qquad \text{(A.11)}$$

The integral in Equation (A.11) is easily evaluated to give

$$Q_F(\rho) = 1 - P_{FA}^{1/(1+\rho)}, \qquad \text{(A.12)}$$

the standard Swerling I result.

APPENDIX B
COMPARISON OF GAUSSIAN AND SINC BEAM PATTERNS

In this appendix, the losses for a horizon search radar employing a sinc pattern are compared to the Gaussian beam results found in the main body of this report.

The gain pattern of a Gaussian beam is

$$G_{\text{Gaussian}} = \exp(-(8\ln 2)\theta^2). \tag{B.1}$$

The sinc beam with the same 6-dB two-way beamwidth is

$$G_{\text{sinc}} = \left[\frac{\sin(2.78\theta)}{2.78\theta}\right]^4. \tag{B.2}$$

Figure B-1 shows the two beam shapes. The major differences are a narrower main beam for the sinc pattern as well as sidelobes that are absent from the Gaussian beam.

The sidelobes should not affect the loss results significantly because the highest sidelobes are down 26 dB from the peak. An extremely high SNR would be required to make the P_d from these sidelobes significant. Because this SNR would be very large in the central beam, the P_d from this beam would be very close to 1 and any additional P_d from the sidelobe would be insignificant.

The width of the central lobe is of more significance due to the much lower gain at the edge of the central lobe where it overlaps with an adjacent beam. Table B-1 shows the two-way gain at the overlap point with the adjacent beam for the α values used in these calculations. For the lower α values (≤ 1), the gain is very slightly higher for the sinc function leading to slightly lower losses. For the higher α values, the difference should be greater with the sinc losses being higher.

Figure B-2 shows the sinc beam losses for a horizon search radar at zero duty factor. This figure is nearly identical to Figure 8(a), the corresponding result for Gaussian beams. The only significant difference occurs at large P_d with large α, giving larger losses for the sinc beam.

There is not a significant difference in the losses between Gaussian and sinc beams for most regions of interest (areas of minimum loss). The approximation of using Gaussian beams appears well justified.

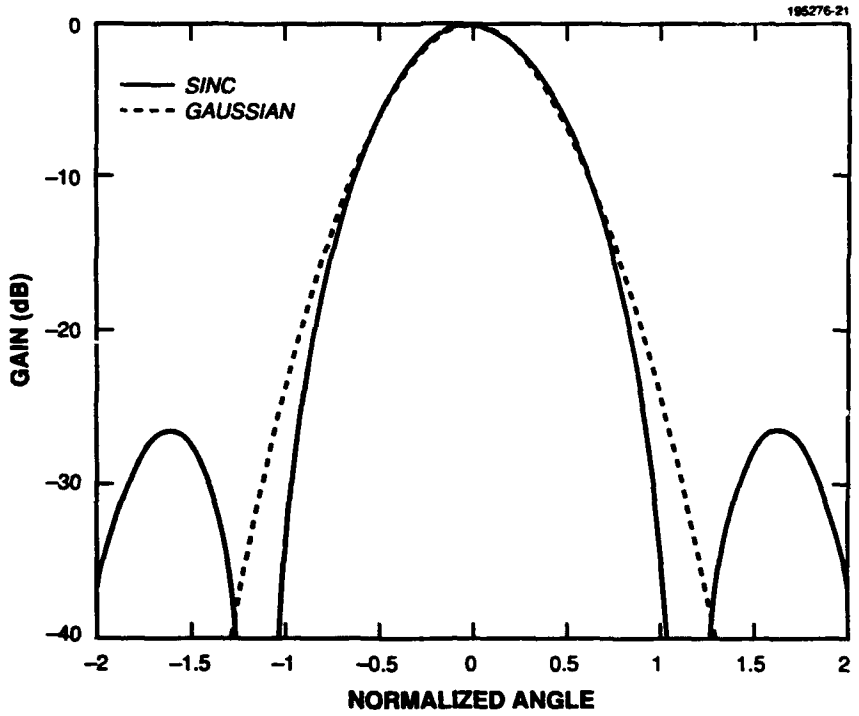

Figure B-1. Gaussian and sinc two-way beam patterns.

TABLE B-1

Two-Way Antenna Gains at Overlap Point with Adjacent Beams

α	G_{Gaussian}	G_{sinc}
0.5	-1.5	-1.4
0.7	-3.0	-2.8
1.0	-6.0	-6.0
1.4	-12.0	-13.1
2.0	-24.0	-35.8

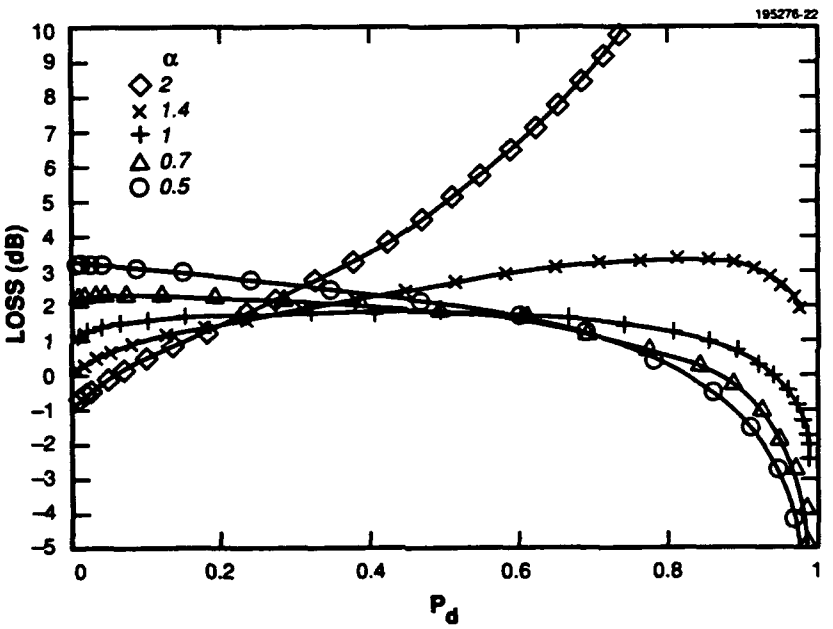

Figure B-2. Losses for horizon search with sinc beams.

REFERENCES

1. L.V. Blake, "The effective number of pulses per beamwidth for a scanning radar," *Proc. IRE 41* (1953), pp. 770-774; Addendum *Proc. IRE 41* (1953), pp. 1785.
2. N.T. Evans and A.J. Kanyuck, "Statistical analysis of antenna pattern loss effects," *IEEE Trans. AES 5*, 77-82 (1969).
3. P.M. Hahn and S.D. Gross, "Beam shape loss and surveillance optimization for pencil beam arrays," *IEEE Trans. AES 5*, 674-675 (1969).
4. G.W. Lank, "Antenna scanning optimization," *IEEE 1980 International Radar Conference*, Arlington, VA, pp 94-99.
5. D.K. Barton and H.R. Ward, *Handbook of Radar Measurements*, Prentice Hall (1969), Appendix A.
6. M. Abromowitz and I.A. Stegun, *Handbook of Mathematical Functions*, National Bureau of Standards (1964).
7. A. Papoulis, *Probability, Random Variables, and Stochastic Processes*, McGraw-Hill (1984), Section 8-3.